Robust propagation of pin-like optical beam through atmospheric turbulence (F)

Ze Zhang (iD), Xinli Liang, Mihalis Goutsoulas, Denghui Li, Xiuting Yang, Shupeng Yin, Jingjun Xu,
Demetrios N. Christodoulides, Nikolaos K. Efremidis, and Zhigang Chen (iD)

COLLECTIONS

F This paper was selected as Featured

View Online   Export Citation   CrossMark

ARTICLES YOU MAY BE INTERESTED IN

Large-scale sharply bending paraxial beams
APL Photonics 4, 056101 (2019); https://doi.org/10.1063/1.5091571

Aberration-insensitive microscopy using optical field-correlation imaging
APL Photonics 4, 066102 (2019); https://doi.org/10.1063/1.5091976
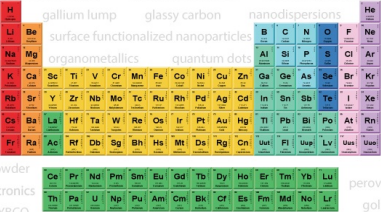
Fourier single-pixel imaging in the terahertz regime
Applied Physics Letters 115, 021101 (2019); https://doi.org/10.1063/1.5094728

Robust propagation of pin-like optical beam through atmospheric turbulence Ⓕ

View Online   Export Citation   CrossMark

Ze Zhang,[1,a)] Ⓘ Xinli Liang,[1] Mihalis Goutsoulas,[2] Denghui Li,[3] Xiuting Yang,[1] Shupeng Yin,[4] Jingjun Xu,[3] Demetrios N. Christodoulides,[5] Nikolaos K. Efremidis,[2,3,6] and Zhigang Chen[3,7,b)] Ⓘ

AFFILIATIONS

[1] Academy of Opto-Electronics, Chinese Academy of Sciences, Beijing 100094, China

[2] Department of Applied Mathematics, University of Crete, Heraklion 71409, Greece

[3] The MOE Key Laboratory of Weak-Light Nonlinear Photonics, TEDA Applied Physics Institute and School of Physics, Nankai University, Tianjin 300457, China

[4] Beijing Institute of Special Electromechanical Technology, Beijing 100012, China

[5] CREOL/College of Optics, University of Central Florida, Orlando, Florida 32816, USA

[6] Institute of Applied and Computational Mathematics, FORTH, 70013 Heraklion, Crete, Greece

[7] Department of Physics and Astronomy, San Francisco State University, San Francisco, California 94132, USA

[a)] zhangze@aoe.ac.cn
[b)] zhigang@sfsu.edu

ABSTRACT

We design and demonstrate what we called shape-preserving "optical pin beams" (OPBs) that possess stable wavefronts against diffraction and ambient turbulence during free-space long distance propagation. Theoretically, we show that a laser beam passing through properly assembled phase elements paired with opposite transverse wavevectors can morph quickly into a stable optical field, exhibiting "self-focusing" dynamics during propagation without optical nonlinearity. The overall shape of such OPBs remains invariant, while their width can in principle be inversely proportional to the propagation distance, in contradistinction to conventional Bessel beams and radially symmetric Airy beams. Experimentally, utilizing a single photoetched mask, we demonstrate efficient generation and robust propagation of the OPB through atmospheric turbulence beyond kilometer distances. We envisage exciting opportunities arising from such OPBs, especially when propagation through turbulent environments is unavoidable.

I. INTRODUCTION

For decades, the prospect of achieving optical stable fields that can propagate invariantly ("diffraction-free" and resilient to perturbations) has been an elusive goal. In space domain, for example, pin-like or needlelike shape-preserving optical beams have always been sought after. Ideally, such optical beams could be exploited for many applications including, for example, remote atmospheric sensing, optical communication, laser guide stars, and lidars. To overcome natural diffraction, one could in principle use linear nondiffract-ing beams (such as Bessel[1–3] and Airy[4–6] beams) or nonlinear optical solitons.[7,8] The former typically requires that the optical beams

carry infinite energy for long enough nondiffracting propagation, while the latter needs an ideal nonlinear hosting medium unsuitable for practical free-space applications. In addition, when an optical beam propagates through turbulent environments, light scattering loss and wavefront distortion have always been an arduous hurdle.[9] To resist the disturbance from ambient turbulence, adaptive optics (AO) has been employed to correct the wavefront distortion. However, due to the complexity of AO systems, it has mainly been used in optical telescopes for astronomical imaging[10] or optical microscopes for biological imaging.[11]

Over the last dozen years, the area of optical beam shaping has attracted tremendous attention, fueled by copious exciting

applications proposed or demonstrated based on self-healing Bessel and Airy beams.[6,12–19] For instance, nondiffracting Bessel beams propagating along a straight line can in principle be exploited for applications in optical communications. Theoretically, it has been shown that Bessel beams have a number of benefits over the conventional Gaussian beams when propagating through atmospheric turbulence.[20] Airy-type accelerating beams, on the other hand, propagate along a curved or self-bending trajectory, also exhibiting nondiffracting and self-healing features while being resilient to perturbations. In recent years, Airy beams or pulses have been highly advocated and tested for a variety of applications, including, for example, particle manipulation, biomedical imaging, material processing, generation of light bullets, and routing of electric discharge and synchrotron radiation.[6] Despite these advances, there are quite a few factors one must consider for using such beams for free-space real applications. First, the propagation distance of nondiffracting beams is very limited in experiment: so far, most of the beam shaping techniques based on spatial light modulators (SLMs) can lead to nondiffracting propagation from only a few centimeters to a few meters even under ideal conditions or with sophisticated designs, although the terms such as "ultralong antidiffracting beam" were used.[14,15,21–23] The intensity structure of these beams cannot be generated efficiently due to the maximum power limit set by the SLM damage threshold. Second, due to the turbulence-induced wavefront distortion, the effectiveness of Bessel and Airy beams is rather limited for applications that require long distance propagation through atmospheric turbulence.[24,25] In addition, even though it has been developed for several decades, AO is still hard to use in free-space applications due to various problems such as technological complexity and high production cost, where the role of propagation-invariant beams of the Airy or Bessel type has yet to be explored.

In this work, we report on the generation of an optical pinlike shape-preserving beam that can propagate in free space (or in the presence of air turbulence) over kilometer distances without significant wavefront distortion, exceeding such light evolution achieved by all previous techniques. To this end, we employ a new mechanism to generate such optical pin beams (OPBs) by eliminating transverse wavevectors with the superposition of directionally truncated Airy-like beam components (see the supplementary material). Directional truncation ensures that all beam components bend toward the center, and thus the main lobe of the beam propagates in a stable fashion. Experimentally, we generate such optical pin beams with a photoetched single fused silica mask and observe robust propagation of high-intensity OPBs in both a laboratory setting and outside free space through atmospheric turbulence. The intensity stability of OPBs is compared directly with a Gaussian beam under the same propagation conditions. In addition, we develop a theoretical model that utilizes radial symmetry to simulate the beam dynamics. Surprisingly, it is found that the beam width decreases in a fashion that is inversely proportional to the propagation distance, and thus the resulting wave takes the form of an optical pin. Clearly, these autofocusing OPBs, as a stable optical wave entity, could be exploited for many applications especially when it is necessary for light to traverse through turbulent media.

II. MATERIALS AND METHODS

The mechanism for highly efficient generation of the shape-preserving OPBs can be understood intuitively from Fig. 1. In particular, Fig. 1(a) illustrates the modulation of a broad beam by an engineered phase mask, leading to cancellation of the transverse wavevectors from pairing opposite mask elements, as detailed in the supplementary material. We all know that a finite sized optical beam can be viewed as consisting of many plane wave components, and its diffraction or wave shape distortion arises from the "dephasing" of these wave components during propagation. To create a beam with shape-preserving characteristics, in the sense that the beam shape does not change during propagation due to diffraction or ambient turbulence, it is necessary to keep all the wave components propagating along the same direction, eliminating any transverse
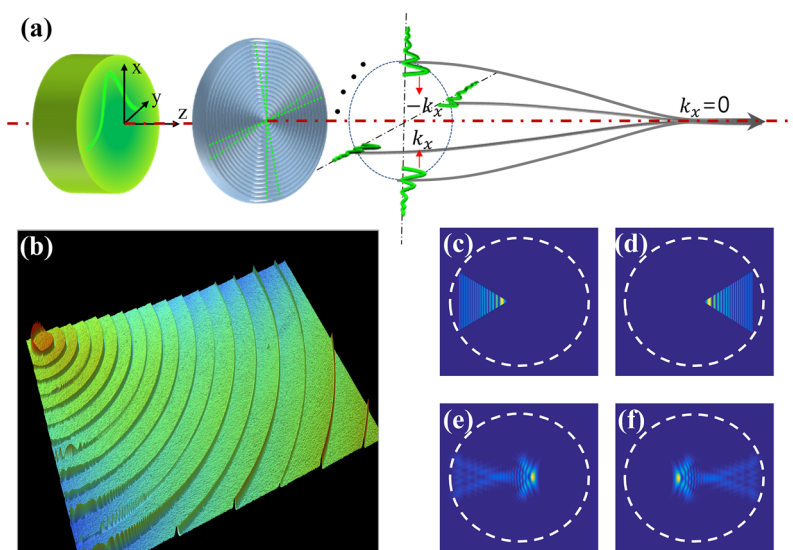
FIG. 1. Illustration of phase engineering for optical pin beam generation. (a) Schematic for generation of shape-preserving OPBs from a single engineered phase mask, where cancellation of transverse wavevectors from two pairs of opposite mask elements is illustrated. (b) Part of the white-light interferogram image of the fabricated 3D mask. [(c)–(f)] Simulations results showing that opposite mask elements [(c) and (d)] lead to opposite directions of energy flow [(e) and (f)] from the side lobes toward the central main lobe.

wavevectors at any longitudinal position. By the virtue of the self-bending property, radially symmetric Airy beams[26–28] are the natural choice for such purpose. As illustrated in Fig. 1(a), two pairs of wave components with Airy-type phase modulation propagate along curved parabolic trajectories, bending toward the center with their transverse wavevectors canceled out. As long as the wavevectors with different bending angles can all undergo such cancellations at different z-positions, a "steady state" nondiffracting propagation can be realized. It should be pointed out that the work here will be focused on the efficient generation of propagation-invariant pinlike optical beams, which is different from the ideal diffraction-free beams whose intensity profile and beam width remain invariant throughout the propagation. In particular, our beam shaping technique is based on a special photoetched mask (rather than an SLM) which allows for 90% conversion efficiency with a low damage threshold.

In experiment, the phase mask is fabricated by use of photolithography for fine-etching a 3D structure with nanometer precision in a quartz plate [Fig. 1(b)], as detailed in the supplementary material. During the etching process, several sets of printing boards are used multiple times to get a series of concentric rings with a jump step of about 40 nm in height. The horizontal scale of these rings ranges from several micrometers to a few millimeters. The exact parameters are so chosen that along any radial direction a cubiclike phase is realized, similar to that of the one-dimensional Airy beams.[4,5] To illustrate the idea of directional truncation of the Airy beam, we numerically truncate a cubic phase pattern for a 1D Airy beam with an isosceles triangle aperture. If we put two such truncated phase filaments in reversed directions as shown in Figs. 1(c) and 1(d), the output beams after phase modulations clearly show bending of their pick intensity toward the center from opposite directions [Figs. 1(e) and 1(f)]. The advantage of such truncation is that the bending or transverse acceleration could be readily adjusted by modifying the apex angle of isosceles phase filaments. Thus, proper assembly of multiple pairs of such phase filaments could lead to a circular phase mask as required for the generation of radially symmetric autofocusing beams. In fact, numerically, we found that if more than 32 such phase filaments are assembled, the generated output beam is quite similar to the abrupt autofocusing beams.[26] As shown in Figs. 1(c)–1(f), the superposition of the

fragmentary Airy beams guarantees the energy flow from the side lobes to the main lobe. Since they propagate along a curved trajectory, different parts of the Airy beams converge at different positions along the propagation direction.

III. EXPERIMENTAL RESULTS AND ANALYSIS

For experimental demonstration of the above proposed OPB, a CW laser operating at 532 nm with an output power of about 2 W was expanded and then sent through a specially engineered photomask, as shown in Fig. 1, as detailed in the supplementary material. The mask has a diameter of about 5 cm, and the measured modulation efficiency of the mask (defined as the ratio of the power of generated OPB at 10 m away to the power of incident Gaussian beam) is about 90%, indicating very good conversion efficiency. A series of experiments were performed both inside laboratory and outside in free space to compare long distance propagation of the laser beam with and without the phase mask. Typical experimental results are presented in Fig. 2, where Figs. 2(a) and 2(b) show the sideview images of the propagation of the normal Gaussian beam (without the mask), and Figs. 2(c) and 2(d) show corresponding images of the optical pin beam generated with the phase mask. The pictures in Figs. 2(a) and 2(c) were taken in a hallway with spread air-borne particles, and those in Figs. 2(b) and 2(d) were taken at about 60 m propagation distance but for another meter long propagation through a container filled with colloidal suspension of polystyrene beads as a scattering medium. From these figures, one can see clearly the pin-like feature of the laser beam with highly localized peak intensity after being modulated by the phase mask [Figs. 2(c) and 2(d)]. A direct comparison of the output intensity profiles between these two beams after propagating 60 m in free space is shown in Fig. 2(e). While the Gaussian beam diffracts slightly and remains to be a broad beam (about 17 mm in diameter), the energy of the OPB becomes highly localized in space (with a FWHM of less than 3 mm), and its peak intensity reaches more than 10 times higher than that of the Gaussian beam after the same 60-m-long propagation distance. In Fig. 3, we show the corresponding transverse intensity patterns and horizontal beam profiles of the OPB taken at different propagation distances while the optimal focus was realized at about 60 m.
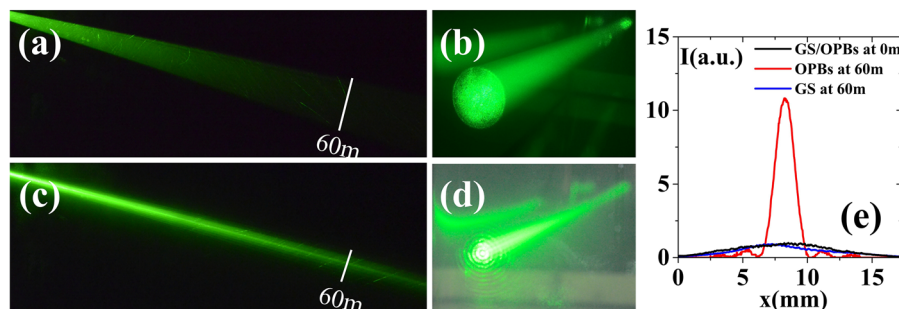
FIG. 2. Experimental side-view comparison between an OPB and a Gaussian beam. Experimental side-view images depicting long distance propagation of [(a) and (b)] a normal Gaussian beam and [(c) and (d)] an optical pin beam generated with the phase mask. Pictures in (a) and (c) were taken for 100 m-long propagation through air in a hallway, and those in (b) and (d) were taken for 1 m-long propagation through colloidal suspension of polystyrene beads. (e) Plots of output intensity profiles for direct comparison between the Gaussian beam (blue) and the OPB (red) after 60 m of propagation.

FIG. 3. Snapshots of the beam profiles from the OPB. Transverse intensity patterns (top row) and corresponding horizontal beam profiles (bottom row) of the optical pin beam taken at different propagation distances (0 m, 2.4 m, 25 m, and 60 m) relative to the mask. Note that the maximum for the y-axis is different for the intensity profiles in the bottom row since the peak intensity for the first two panels is much lower than that for the last two panels (note that the images in the last two panels w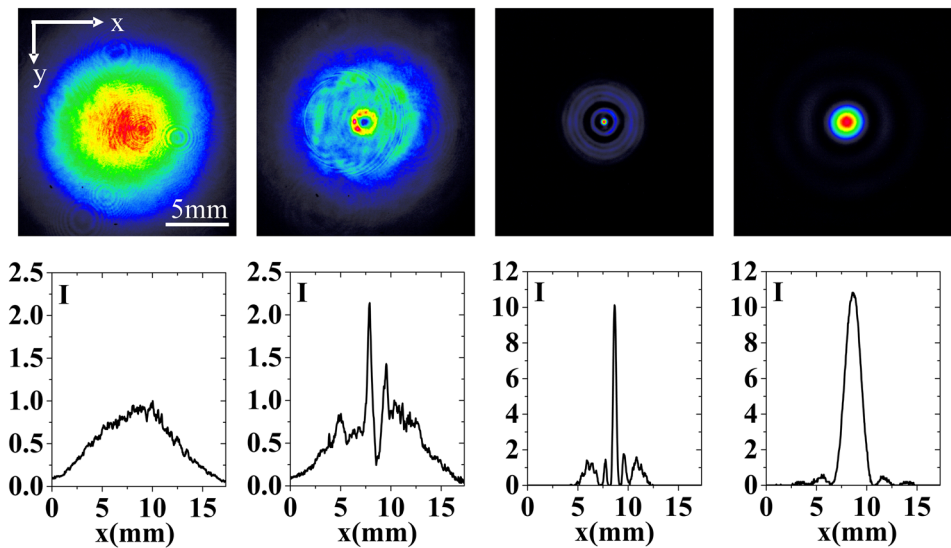ere taken with a stronger attenuation to avoid camera saturation). These figures are meant to show qualitatively that the peak intensity of the OPB increases and the overall beam width decreases with the propagation distance.

Perhaps, the most exciting experimental results are those shown in Fig. 4 (see videos in the supplementary material), where a direct comparison is displaced for the intensity pattern and its stability between a normal Gaussian beam and an OPB after more than 1 km of propagation through atmospheric turbulence. As clearly seen in the pictures of Figs. 4(a) and 4(b) taken in open country, the overall pattern of the OPB takes a Bessel-like circular shape with a pronounced main lobe, and its width only increased just a few millimeters during propagation (from 6 mm when close to the mask to 9 mm after 1 km long propagation). In contrast, the Gaussian beam with the same output size/power from the laser expands and fluctuates dramatically due to diffraction and ambient disturbance through atmosphere. While it is apparent that the OPB has evolved into a Bessel-like intensity pattern [Fig. 4(b)] at such a kilometer long distance, one must keep in mind that, up to now, Bessel beams have been realized only with a few meters in length with currently available techniques even under ideal conditions. In an ideal design, as we should discuss later in theory, one could in principle move the "focus" to much longer distances, which could lead to desirable applications of these optical beams when transmission through free-space must be considered. In the supplementary material, detailed simulation results are given to show that, for long distance
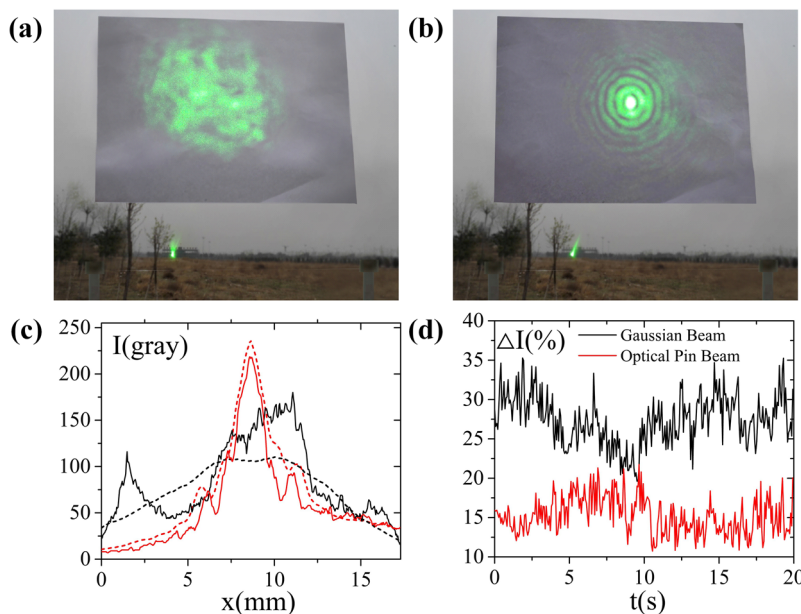
FIG. 4. Experimental demonstration of robust propagation of the OPB through atmospheric turbulence (see videos in the supplementary material). [(a) and (b)] Direct comparison of laser beam intensity patterns between (a) a normal Gaussian beam (without mask) and (b) an OPB (with mask) after propagation over 1 km distance in open country. The main lobe of the OPB has a width of about 9 mm, while the Gaussian beam spreads to about 17 cm and fluctuates dramatically. The laser source is visible afar in the lower bottom corner. [(c) and (d)] Comparison of spatial and temporal stability of the OPB and the Gaussian beam after propagation for 45 m through turbulent air in a lab room driven by a central air conditioner. (c) Transverse intensity profiles for the Gaussian (black curves) and the OPB (red curves) and (d) their corresponding relative intensity variation as a function of time. The intensity plots in (c) and (d) are in arbitrary units for stability analysis rather than measurement of absolute power.

propagation, the OPB has advantages over the Bessel beam under the same conditions in terms of preserving the peak intensity and the focused beam profile.

Furthermore, to compare directly the robustness of the OPB with the Gaussian beam, we let both beams propagate through turbulent air inside a lab room driven by a central air conditioner at maximum strength. The recorded beam patterns after 45 m of propagation are used to analyze the intensity stability, as shown in Figs. 4(c) and 4(d). Evidently, the OPB exhibits a robust intensity stability while localized in space as compared to their Gaussian counterparts. In Fig. 4(c), the spatial intensity profile recorded at a given time (red solid curve) matches well with the time-averaged intensity profile (red dashed curve) for the OPB. Contrarily, for the Gaussian beam, the intensity profile at a given time (black solid curve) deviates substantially with the time-averaged intensity profile (black dashed curve). In addition, in Fig. 4(d), we plot the percentage of the intensity variation across a beam diameter with time, defined as

$$\Delta I_t = \frac{\int |I(x,y,t) - I_{mean}(x,y)| dxdy}{\int I_{mean}(x,y) dxdy}, \tag{1}$$

where the time average is performed from 290 frames taken over 20 s. Clearly, these results show that the intensity variation with time of the OPB is significantly less as compared to that of the Gaussian beam. From both the spatial intensity profile and the percentage of the intensity variation with time, we can conclude that the power of the OPB is much more localized in space and meanwhile has much less fluctuation in time. Thus, apart from the antidiffracting feature, we have experimentally demonstrated that the OPB represents an optical stable shaped light field that can undergo robust propagation through atmosphere turbulence. As mentioned before, this can be understood from the structure of the transverse wavevectors: the influence of air turbulence to a laser beam is in some sense to introduce random transverse wavevectors, which during the propagation can be canceled out continuously at different distances for an OPB, thus maintaining its intensity distribution. It is also worth pointing

out that, compared with an AO system, our method for generation of a turbulence-resistant optical beam does not need feedback from a closed control loop and thus could be readily implemented in practical application systems.

To better understand the underlying mechanism for the generation of the demonstrated OPB, we have numerically studied the formation of such autofocusing Bessel-like beams by assembling multiple phase elements in pairs that lead to opposite transverse wavevectors. Each pair of the elements corresponds to two Airy-like fragments bending toward the center but from opposite directions. The resulting beam thus appears to focus after certain propagation distances (Fig. 5). However, it is found that when the number of elements is increased to 32, the resulting beam matches almost perfectly with a radially symmetric Airy beam [Fig. 5(b)]. In contrast to the previously demonstrated abruptly autofocusing Airy beams,[26–28] such synthetic OPBs do not start with a broad ring beam but rather morph into a Bessel-like profile fairly quickly right after the input plane, although optimal "focusing" occurs in later propagation, as shown in Figs. 5(c)–5(e).

Theoretically, we can describe the dynamics of the system by considering the case where the number of the Airy-type fragments goes to infinity. In this case, the dynamics of the optical beam in the paraxial limit is given by the following Fresnel integral:

$$\psi(r,z) = \frac{ke^{\frac{ikr^2}{2z}}}{iz} \int_0^\infty \psi_0(\rho) J_0\left(\frac{kr\rho}{z}\right) e^{\frac{ikr^2}{2z}} d\rho, \tag{2}$$

where $\psi_0(\rho)$ is the optical beam at the input ($z = 0$) or the phase mask plane, $k = 2\pi/\lambda$ is the wavenumber, and J_0 is the zeroth order Bessel function. We assume an initial condition with the Airy-type phase (proportional to $\rho^{\frac{3}{2}}$)

$$\psi_0(\rho) = A(\rho) e^{-i\frac{4}{3}k\beta^{\frac{1}{2}}\rho^{\frac{3}{2}}}, \tag{3}$$

where β is a parameter with inverse length dimensions that determines the local frequency of the phase oscillations of the wave. Following a stationary phase approach similar to the one used to derive
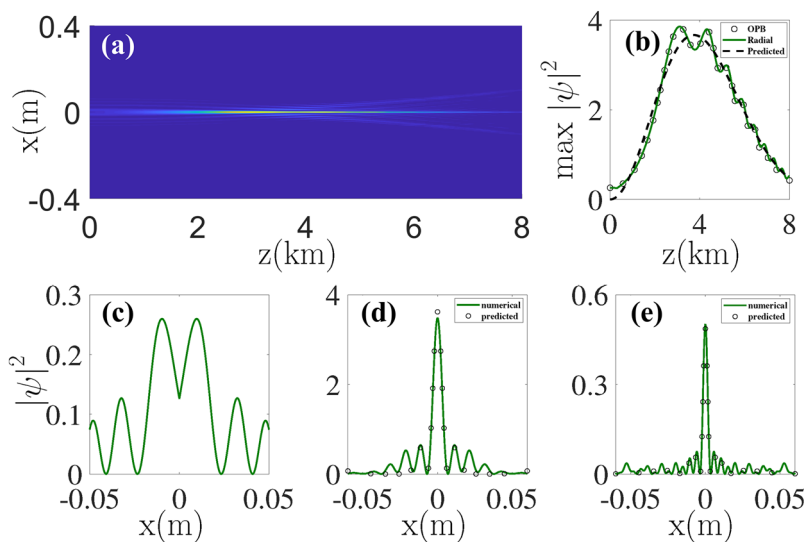
FIG. 5. Numerical simulation showing long distance propagation of the OPB. (a) Side-view of the OPB propagating 8 km, where optimal "focusing" occurs around z = 5.0 km. (b) Peak intensity comparison of a modulated OPB with 32 "fragmented" phase filaments, a radially symmetric Airy beam, and the theoretical prediction. [(c)–(e)] Intensity profiles taken at z = 0, 4, and 8 km and comparison theory. The theoretical results are obtained using Eq. (4) and are in very good agreement with the numerical simulations.

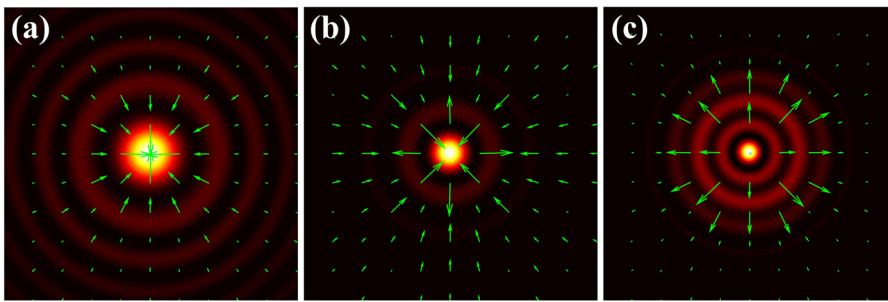**FIG. 6**. Calculated energy flow of the OPB during propagation. [(a)–(c)] Poynting vector distribution at different propagation distances of z = 30, 60, and 90 m. A balanced energy flow is reached after about 60 m of propagation.

Eq. (23) of Ref. 39 (see also the supplementary material) to the above Hankel transform, we conclude that the dynamics of the optical wave is given by

$$\psi(r,z) = 8\left(\pi k \beta^2 z^3\right)^{\frac{1}{2}} A\left(4\beta z^2\right) J_0\left(4k\beta\rho z\right) e^{i\Phi}, \tag{4}$$

where $\Phi = \frac{kr^2}{2z} - \frac{8}{3}k\beta^2 z^3 - \frac{\pi}{4}$. We see that the resulting wave takes the form of a Bessel-like beam with width that is inversely proportional to the propagation distance

$$W(z) = \frac{1}{4k\beta z}. \tag{5}$$

Following a series of numerical simulations, we have found that our theoretical calculations are very accurate in describing the dynamics of the OPBs.

To show that the OPB has a robust intensity profile of the main lobe during propagation, we calculated the Poynting vector distribution or the energy flow in the transverse plane at different propagation distances (Fig. 6). After 60 m of propagation, there is already a good balance for the main lobe between the inward and outward flows. At 90 m of propagation, there is little energy flow in any transverse direction for the main lobe, indicating that the energy flow in the main lobe has somewhat reached a quasi-steady state, although there is still outward energy flow for the side lobes.

Finally, we want to mention that, in this work, we focused on reporting mainly the experimental generation of the OPBs and their robust free-space propagation through atmospheric turbulence. We did not present rigorous numerical/theoretical modeling of the effect from Kolmogorov turbulence, where the dependency of the linear refraction index on statistical fluctuation (characteristic of the local turbulence) is important.[40–42] Such an issue certainly merits further studies. Numerically, we used the phase screen method to simulate turbulent phase structure on the OPB and the effects of turbulence with different strengths. These results are presented in the supplementary material, showing that even under turbulent environments the OPB still exhibits decent antidiffracting and turbulence-resisting features, indicating the robustness of such beams as observed in our experiments.

IV. CONCLUSION

In summary, we have experimentally demonstrated the generation of antidiffracting optical pin beams, along with their robust long distance propagation through artificial turbulent air as well as over kilometric distances through real-world atmosphere turbulence. The advantages of such OPBs over conventional Gaussian beams were also illustrated. Compared with previously demonstrated Bessel beams and radially symmetric Airy beams, we show that numerically the OPBs can exhibit the autofocusing feature along straight-line propagation with their peak energy delivered to over kilometers in free space. While recent efforts have led to the generation of a variety of shaped light in space and time, such as Bessel-type optical bullets,[29] needlelike electromagnetic wavepackets,[30] and even space-time light sheets and pulsed beams,[21,22] our results may bring about a novel approach for designing laser beams with turbulence-resistant features for various applications when traversing through atmospheric turbulence is unavoidable. Compared with adaptive optics, our method may prove to be feasible for free-space communication applications with turbulence-resistant optical beams. In addition, we believe that the results demonstrated here may prove to be relevant to shaped optical wavepackets in disordered photonics proposed and tested for imaging and focusing in scattering biological media,[31–36] as well as to fine-shaped beam for writing scalable optical waveguides and photonic lattices.[37,38]

SUPPLEMENTARY MATERIAL

See supplementary material for phase mask design, experimental setup, supplemental videos and details of numerical simulation.

REFERENCES

[1] J. Durnin, J. Opt. Soc. Am. A **4**, 651 (1987).
[2] J. Durnin, J. J. Miceli, Jr., and J. H. Eberly, Phys. Rev. Lett. **58**, 1499 (1987).
[3] D. McGloin and K. Dholakia, Contemp. Phys. **46**, 15 (2005).
[4] G. A. Siviloglou and D. N. Christodoulides, Opt. Lett. **32**, 979 (2007).
[5] G. A. Siviloglou, J. Broky, A. Dogariu, and D. N. Christodoulides, Phys. Rev. Lett. **99**, 213901 (2007).
[6] N. K. Efremidis, Z. Chen, M. Segev, and D. N. Christodoulides, Optica **6**, 686 (2019).
[7] Y. S. Kivshar and G. Agrawal, *Optical Solitons: From Fibers to Photonic Crystals* (Academic, Boston, MA, 2003).

[8] Z. Chen, M. Segev, and D. N. Christodoulides, Rep. Prog. Phys. **75**, 086401 (2012).

[9] L. C. Andrews and R. L. Phillips, *Laser Beam Propagation Through Random Media* (SPIE Press, Bellingham, WA, 1998).

[10] R. Davies and M. Kasper, Annu. Rev. Astron. Astrophys. **50**, 305 (2012).

[11] M. J. Booth, Light: Sci. Appl. **3**, e165 (2014).

[12] A. Dudley, M. Lavery, M. Padgett, and A. Forbes, Opt. Photonics News **24**, 22 (2013).

[13] F. O. Fahrbach, P. Simon, and A. Rohrbach, Nat. Photonics **4**, 780 (2010).

[14] M. Duocastella and C. B. Arnold, Laser Photonics Rev. **6**, 607 (2012).

[15] S. Akturk, B. Zhou, M. Franco, A. Couairon, and A. Mysyrowicz, Opt. Commun. **282**, 129 (2009).

[16] B. Hadad, S. Froim, H. Nagar, T. Admon, Y. Eliezer, Y. Roichman, and A. Bahabad, Optica **5**, 551 (2018).

[17] J. Nylk, K. McCluskey, M. A. Preciado, M. Mazilu, Z. Yang, F. J. Gunn-Moore, S. Aggarwal, J. A. Tello, D. E. K. Ferrier, and K. Dholakia, Sci. Adv. **4**, eaar4817 (2018).

[18] M. Clerici, Y. Hu, P. Lassonde, C. Milián, A. Couairon, D. N. Christodoulides, Z. Chen, L. Razzari, F. Vidal, F. Légaré, D. Faccio, and R. Morandotti, Sci. Adv. **1**, e1400111 (2015).

[19] M. Henstridge, C. Pfeiffer, D. Wang, A. Boltasseva, V. M. Shalaev, A. Grbic, and R. Merlin, Science **362**, 439 (2018).

[20] P. Birch, I. Ituen, R. Young, and C. Chatwin, J. Opt. Soc. Am. A **32**, 2066 (2015).

[21] H. E. Kondakci and A. F. Abouraddy, Phys. Rev. Lett. **120**, 163901 (2018).

[22] B. Bhaduri, M. Yessenov, and A. F. Abouraddy, Opt. Express **26**, 20111 (2018).

[23] X. Weng, Q. Song, X. Li, X. Gao, H. Guo, J. Qu, and S. Zhuang, Nat. Commun. **9**, 5035 (2018).

[24] W. Nelson, J. P. Palastro, C. C. Davis, and P. Sprangle, J. Opt. Soc. Am. A **31**, 603 (2014).

[25] N. Mphuthi, R. Botha, and A. Forbes, J. Opt. Soc. Am. A **35**, 1021 (2018).

[26] N. K. Efremidis and D. N. Christodoulides, Opt. Lett. **35**, 4045 (2010).

[27] D. G. Papazoglou, N. K. Efremidis, D. N. Christodoulides, and S. Tzortzakis, Opt. Lett. **36**, 1842 (2011).

[28] P. Zhang, J. Prakash, Z. Zhang, M. S. Mills, N. K. Efremidis, D. N. Christodoulides, and Z. Chen, Opt. Lett. **36**, 2883 (2011).

[29] P. Panagiotopoulos, D. G. Papazoglou, A. Couairon, and S. Tzortzakis, Nat. Commun. **4**, 2622 (2013).

[30] L. J. Wong and I. Kaminer, ACS Photonics **4**, 1131 (2017).

[31] D. S. Wiersma, Nat. Photonics **7**, 188 (2013).

[32] S. Popoff, G. Lerosey, M. Fink, A. C. Boccara, and S. Gigan, Nat. Commun. **1**, 81 (2010).

[33] I. M. Vellekoop, A. Lagendijk, and A. P. Mosk, Nat. Photonics **4**, 320 (2010).

[34] O. Katz, E. Small, Y. Bromberg, and Y. Silberberg, Nat. Photonics **5**, 372 (2011).

[35] A. P. Mosk, A. Lagendijk, G. Lerosey, and M. Fink, Nat. Photonics **6**, 283 (2012).

[36] O. Katz, E. Small, Y. Guan, and Y. Silberberg, Optica **1**, 170 (2014).

[37] S. Xia, A. Ramachandran, S. Xia, D. Li, X. Liu, L. Tang, Y. Hu, D. Song, J. Xu, D. Leykam, S. Flach, and Z. Chen, Phys. Rev. Lett. **121**, 263902 (2018).

[38] F. Xin, M. Flammini, F. D. Mei, L. Falsi, D. Pierangeli, A. J. Agranat, and E. DelRe, Phys. Rev. Appl. **11**, 024011 (2019).

[39] M. Goutsoulas and N. K. Efremidis, Phys. Rev. A **97**, 063831 (2018).

[40] V. P. Kandidov, O. G. Kosareva, M. P. Tamarov, A. Brodeur, and S. L. Chin, Quantum Electron. **29**, 911 (1999).

[41] S. L. Chin, A. Talebpour, J. Yang, S. Petit, V. P. Kandidov, O. G. Kosareva, and M. P. Tamarov, Appl. Phys. B **74**, 67 (2002).

[42] R. Ackermann, G. Méjean, J. Kasparian, J. Yu, E. Salmon, and J. P. Wolf, Opt. Lett. **31**, 86 (2006).